Weierstraß-Institut
für Angewandte Analysis und Stochastik

im Forschungsverbund Berlin e.V.

Preprint ISSN 0946 – 8633

PID-Control of Laser Surface Hardening of Steel

Dietmar Hömberg[1] and Wolf Weiss[2]

submitted: 13th October 2003

[1] E-Mail: hoemberg@wias-berlin.de [2] E-Mail: weiss@wias-berlin.de

No. 876
Berlin 2003

2000 *Mathematics Subject Classification.* 35K05,93C20.

Key words and phrases. Feedback Control, Heat Treatment, Phase Transitions.

This work has been supported by the DFG Research Center "Mathematics for key technologies" (FZT 86) in Berlin.

Edited by
Weierstraß-Institut für Angewandte Analysis und Stochastik (WIAS)
Mohrenstraße 39
D — 10117 Berlin
Germany

Fax: + 49 30 2044975
E-Mail: preprint@wias-berlin.de
World Wide Web: http://www.wias-berlin.de/

Abstract

We discuss control strategies for the laser surface hardening of steel. The goal is to acchieve a prescribed hardening depth avoiding surface melting. Our mathematical model consists of a system of ODEs for the phase volume fractions coupled with the heat equation. The system is solved semi-implicitely using the finite element method. To obtain a uniform hardening depth the first attempt is to use PID control to achieve a constant temperature in the hot spot of the laser beam on the surface. However, the numerical results prove that this is not sufficient. We show that the best strategy is to control the temperature close to the lower boundary of the hardening zone. Then one can compute the optimal temperature in the hot spot of the beam and use it as the set-point for the pyrometer control of the real process.

1 Introduction

In most structural components in mechanical engineering, the surface is particularly stressed. For components made of steel a heat treatment by a laser beam may be used to increase the hardness of the outer surface. The typical depth of such a hardening zone lies between 0.3 and 1.0 mm.

Figure 1 depicts the process of laser surface hardening. A laser beam moves along the workpiece surface. The absorbed laser energy leads to a heating of the boundary layer and a subsequent growth of austenite, the high-temperature phase in steel. If the workpiece volume is big enough, during the self-cooling of the workpiece the austenite will be completely transformed to martensite, a steel phase which is characterized by great hardness. Otherwise, also other phases like ferrite, pearlite and bainite can be produced, which are more ductile and less hard [2].

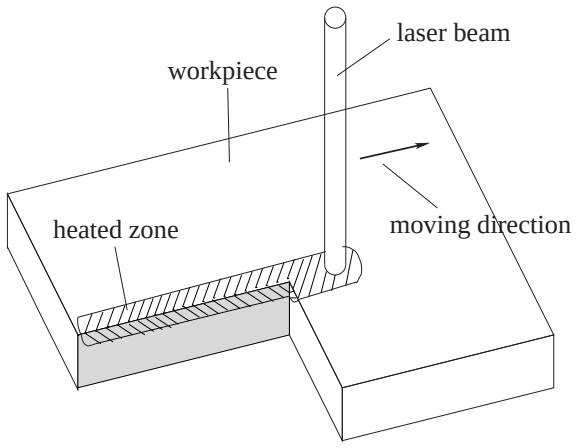

Figure 1: Sketch of laser surface hardening.

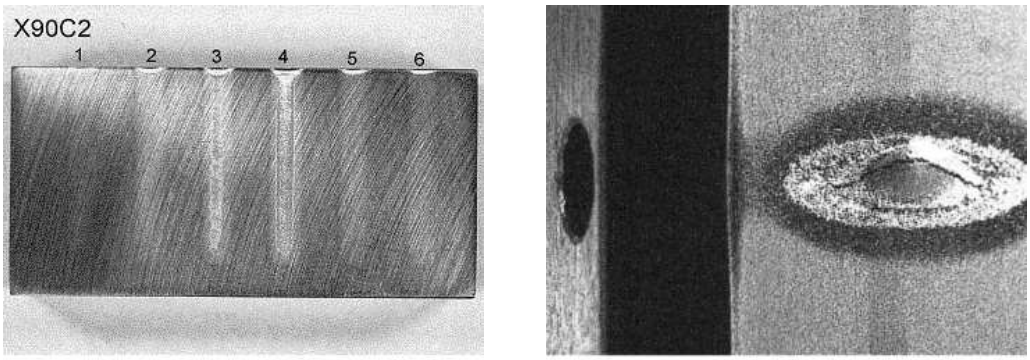

Figure 2: Effects of laser hardening with constant energy and velocity: over-heating and surface melting close to workpiece edge (left) and above holes inside the workpiece (right).

Figure 2 shows why there is a demand for precise process control in laser surface hardening. On the left one can see 6 tracks of a laser hardening, each with different (but constant) laser energy and velocity. While the middle part of each of the laser tracks looks rather stationary one can observe a thickening of the track around the edge where the laser leaves the surface. In some of the tracks this is accompanied by a melting of the surface. To avoid this over-heating effect, it is important to reduce the laser energy when the beam approaches a workpiece edge. The same can happen if the workpiece thickness changes below the laser track. Figure 2 (right) shows the effect of a cylindrical hole parallel to the workpiece surface and perpendicular to the laser track. Here, even a bursting of the surface can be observed. Again, it would be desirable to have an automatic process control which reduces the laser energy when crossing the hole.

The paper is organized as follows. In Section 2 we describe a mathematical model for the surface hardening of steel, consisting of a system of ordinary differential equations for the evolution of phase transitions coupled with a quasi-linear heat equation. In Section 3 we investigate the interplay of different control parameters and present numerical simulations for the complete nonlinear system.

Section 4 is devoted to PID process control for laser hardening. The last section is concerned with some concluding remarks about the interplay between numerical simulations and process control of the hardening machine.

2 Mathematical modeling

2.1 Phase transitions

The basic assumption for our modeling approach is that all the information about the evolution of phase transitions in steel is contained in the isothermal and non-isothermal time-temperature-transformation (TTT-) diagrams of the respective steel

[2]. Thus we do not attempt to derive a model where each factor can be given a precise physical meaning. Instead our goal has been to develop a phenomenological model and a procedure of parameter identification such that the transformation diagrams can be reproduced very well. Our approach is based on the model by Leblond and Devaux [8]. However, compared to the Leblond-Devaux approach our model has more degrees of freedom.

In the sequel, let $T(x,t)$ be a temperature-field with time–derivative $\dot{T}$. The volume fractions of austenite, ferrite, pearlite, bainite and martensite are denoted by a, f, p, b and m. To be more precise, f, p, b and m are relative volume fractions describing that portion of ferrite, pearlite, bainite and martensite, respectively, which has been transformed from the austenite fraction produced during heating. The expression $[u]_+$ describes the positive part of u, i.e.

$$[u]_+ = \max\{u\,,\,0\}.$$

Then we consider the following general model of phase transitions during one heat treatment cycle of heating and cooling:

$$a(0) = 0,\ f(0) = f_0,\ p(0) = p_0,\ b(0) = b_0,\ m(0) = 0 \tag{1a}$$

$$\dot{a}(t) = \frac{1}{\tau_a(T)}\Big[a_{eq}(T) - a\Big]_+ - \dot{f} - \dot{p} - \dot{b} - \dot{m} \tag{1b}$$

$$\dot{f}(t) = f^{r_f(T)}\Big[\tilde{f}_{eq}(T) - f\Big]_+^{s_f(T)} g_f(T) h_f(\dot{T}) \tag{1c}$$

$$\dot{p}(t) = p^{r_p(T)}\Big[\tilde{p}_{eq}(T) - p\Big]_+^{s_p(T)} g_p(T) h_p(\dot{T}) \tag{1d}$$

$$\dot{b}(t) = b^{r_b(T)}\Big[\tilde{b}_{eq}(T) - b\Big]_+^{s_b(T)} g_b(T) h_b(\dot{T}) \tag{1e}$$

$$\dot{m}(t) = \frac{1}{\tau_m(T)}\Big[\tilde{m}(T) - m\Big]_+. \tag{1f}$$

The functions $\tilde{f}$, $\tilde{p}, \tilde{b}$ and $\tilde{m}$ are defined by

$$\tilde{f}_{eq}(T) = \min\{f_{eq}(T), a - p - b - m\} \tag{2a}$$

$$\tilde{p}_{eq}(T) = \min\{p_{eq}(T), a - f - b - m\} \tag{2b}$$

$$\tilde{b}_{eq}(T) = \min\{b_{eq}(T), a - f - p - m\} \tag{2c}$$

$$\tilde{m}(T) = \min\{m_{KM}(T), a - f - p - b\} \tag{2d}$$

The equilibrium volume fractions a_{eq}, f_{eq}, p_{eq} and b_{eq} can be derived from the respective isothermal TTT-diagram. The function m_{KM} describes the volume fraction of martensite according to the Koistinen and Marburger formula [7], i.e.,

$$m_{KM}(T) = 1 - e^{-c_{km}(M_s - T)},$$

where c_{km} and M_s again can be drawn from the respective TTT-diagram. Eqns. (2a)–(2d) reflect the fact that the real equilibrium volume fraction of one phase

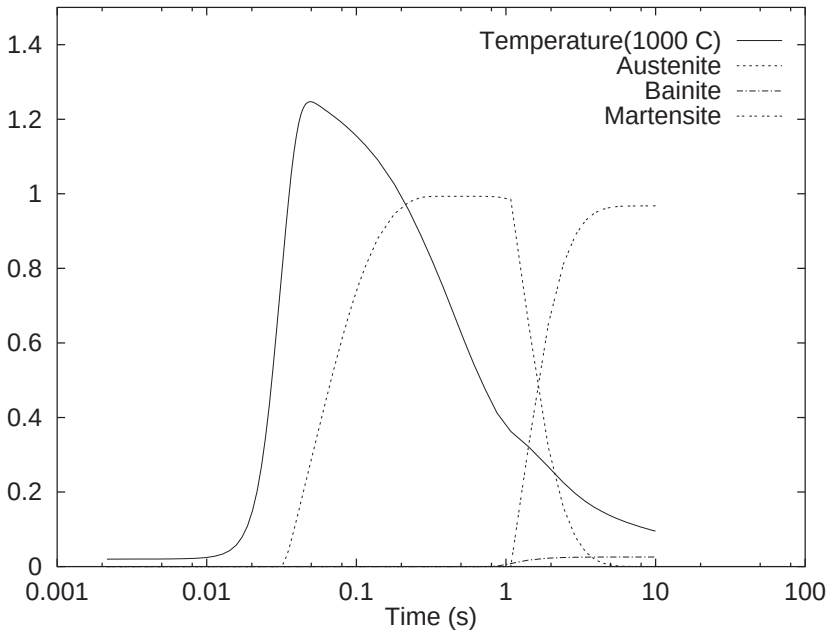

Figure 3: Typical evolution of temperature and the evolution of volume fractions as the solution to (1)–(2) during surface hardening.

cannot exceed the remaining part of austenite, which has not been transformed to another phase.

For the temperature dependent exponents r_f, s_f, r_p, s_p, r_b, s_b, g_f, g_p, and g_b, we have derived identification tools based on a repeated solution of the system (1) for isothermal transformation diagrams. In the non-isothermal case the onset of transfomations is moved to later time and lower temperature. This effect is described by the factors $h_f(\dot{T})$, $h_p(\dot{T})$ and $h_b(\dot{T})$ which have to be identified from the non-isothermal diagrams. Especially, in the case of an isothermal transformation (i.e. $\dot{T} = 0$) these coefficients have to satisfy

$$h_f = h_p = h_b = 1.$$

In an interdisciplinary project with materials scientists and industrial partners, we have identified the necessary model parameters for a number of steels relevant for beam surface hardening. The results are documented in [1].

Except for the introduction of the positive-part function $[\,.\,]_+$, the first part of (1b) is the original formula of Leblond and Devaux [8]. The equilibrium fraction a_{eq} is zero below a threshold temperature A_s and 1 above another threshold temperature A_f. Inbetween it grows monotonically. Hence, with growing temperature, the growth of austenite begins, when the A_s temperature is reached. Upon cooling, owing to the positive part function $[.]_+$, the first term in (1b) gives no contribution. The austenite fraction is decreased due to the growth of the other phases. Note that one has to assume strictly positive initial conditions for ferrite, pearlite and bainite in order to obtain a unique solution to (1)–(2). Figure 3 shows a typical evolution

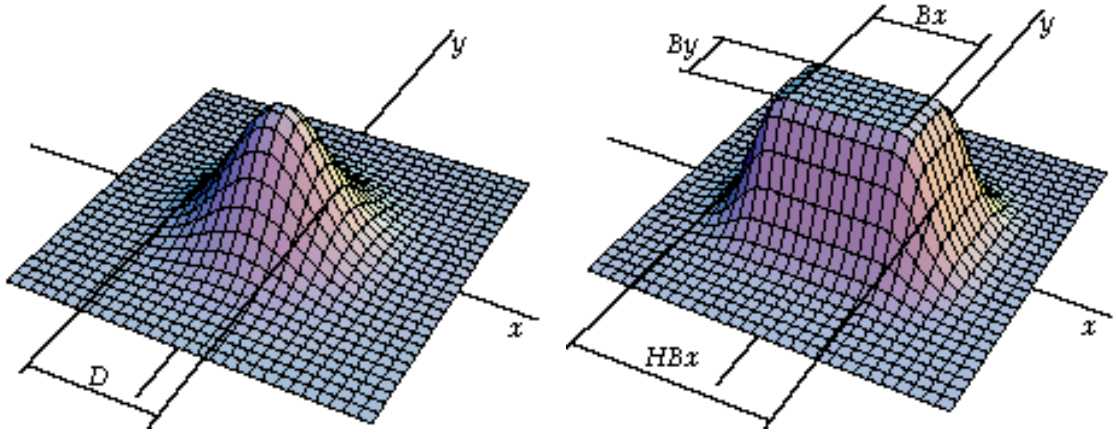

Figure 4: Radiation profiles of a gas laser (left) and a solid state laser (right).

of temperature and the evolution of volume fractions as the solution to (1)–(2) during surface hardening.The first curve from the left is the evolution of temperature. Because of the heating, austenite starts to grow which is dissolved into martensite and a small amount of bainite.

2.2 Heat conduction

To obtain the temperature evolution one has to solve the energy balance equation

$$\rho c(T)\dot{T} - \nabla \cdot \Big(k(T)\nabla T\Big) = q, \tag{3a}$$

where the heat source q stems from the latent heats L of the respective phase transitions and is given by

$$q = \rho\Big(- L_a\dot{a} + L_f\dot{f} + L_p\dot{p} + L_b\dot{b} + L_m\dot{m}\Big). \tag{3b}$$

The initial and boundary conditions are

$$T(0) = T_0 \tag{3c}$$

$$-k(T)\frac{\partial T}{\partial n} = \kappa\mathcal{F}. \tag{3d}$$

Here κ is the absorption coefficient, $\mathcal{F}$ the radiation flux, ρ the density, c specific heat, k the heat conductivity and $\frac{\partial T}{\partial n}$ the normal derivative of T.

The radiation flux $\mathcal{F}$ is a product of radiation power G and a normalized radiation profile $\mathcal{F}_0$, i.e.,

$$\mathcal{F}(x,t) = G(t)\,\mathcal{F}_0(x - v\,t). \tag{4}$$

The radiation power G will serve as the control variable in the sequel. The velocity vector v (assumed constant to simplify the exposition) describes the movement of

the heat source on the workpiece surface. Figure 4 depicts the Gaussian profile of a gas laser (left) and the rectangularly shaped profile of a solid state laser. Instead of laser beams it is also possible to use electron beams which may have much more complicated radiation profiles.

Since self-cooling of the workpiece is the main effect in laser surface treatments, we neglect cooling through the surface. Hence on parts of the surface that are not penetrated by laser, we obtain from (3d) the adiabatic condition

$$\frac{\partial T}{\partial n} = 0.$$

The complete mathematical problem of surface hardening consists in finding a solution to the coupled system (1)–(3). The specific mathematical difficulty lies in the nonlinearities in $\dot{T}$, the time-derivative of temperature. However, for a mathematical problem with similar nonlinearities, the existence of a unique solution has already been proved [6].

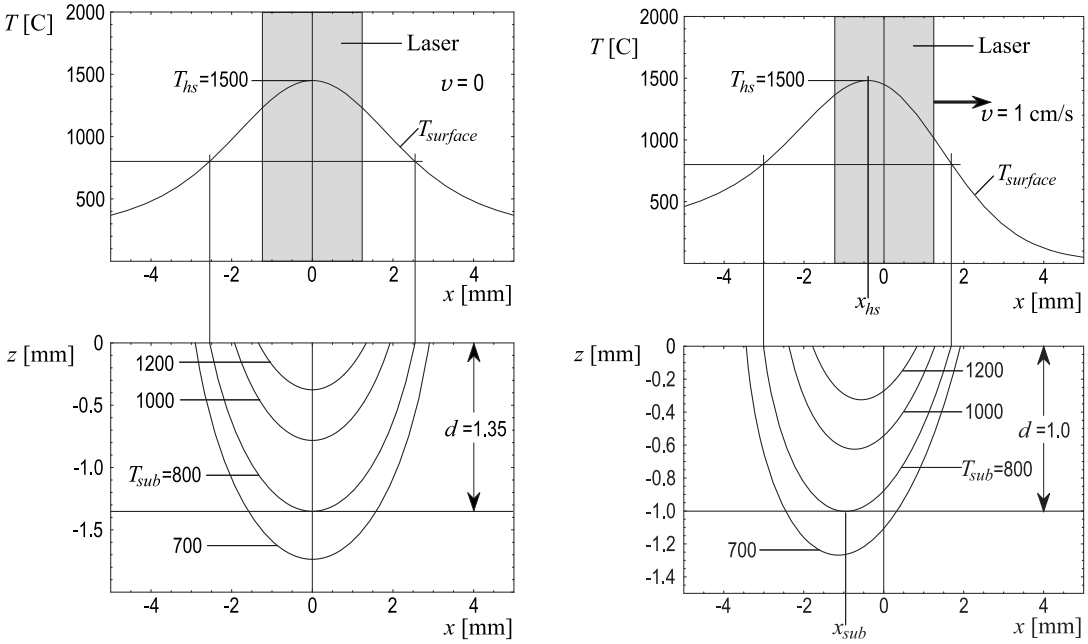

Figure 5: Temperature profile corresponding to a Gaussian intensity profile. Left: laser at rest. Right: Moving with constant velocity.

3 Numerical simulations

3.1 Interplay of control parameters

The principal shape of the intensity profile is determined by the choice of the laser type, i.e. gas or solid-state laser. The remaining control parameters are the moving

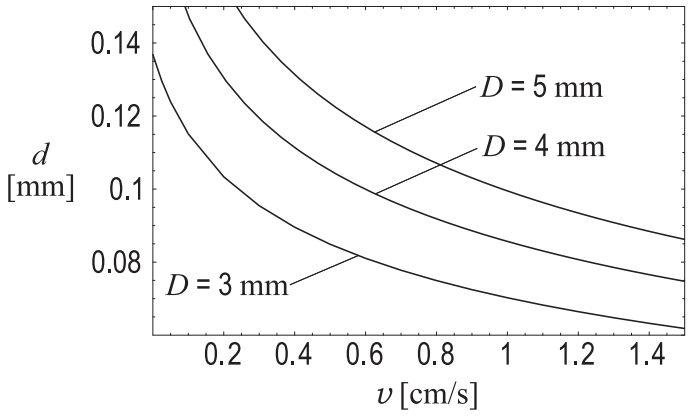

Figure 6: Relation between hardening depth and moving velocity.

velocity v and the laser power G. To obtain some informations about the interplay between velocity and power to realize a desired hardening depth we have performed some parameter studies for (3). We have restricted ourselves to the special situation of the half-space, where the heat source has a Gaussian shape corresponding to a gas laser (cf. Figure 4, left) and is moving with constant velocity. In this quasistatic case an explicit solution is at hand [5].

Figure 5 depicts the temperature profile corresponding to a gas laser with Gaussian intensity distribution and a beam diameter D of 3 mm. For a laser at rest (top), the temperature isolines are centered symmetrically around the middle line of the laser beam. For a moving laser (bottom) the isolines lag behind the middle line of the laser beam. Moreover, the threshold temperature A_s to produce the high temperature phase austenite, which is $A_s = 800^oC$ in this example, is reached in a distance $d = 1.35mm$ for a laser at rest, but only $d = 1.0mm$ for the moving laser. Hence the parameter d may serve as an upper bound for the maximal hardening depth that can be obtained for a given laser velocity.

Figure 6 shows how d decreases with increasing velocity. The laser power is adjusted in such a way that the temperature remains just below the melting point. The three curves correspond to three different beam diameters D. In particular, one can conclude that there is a maximal velocity v for each desired hardening depth, which must not be exceeded.

3.2 Influence of geometry

To investigate the influence of geometry on the hardening profile we have performed numerical simulations for the complete nonlinear mathematical model. For details about the numerical algorithm we refer to [2]. We only want to mention here that it is indispensable to use an implicit discretization for the nonlinearities in $\dot{T}$ in order to obtain a stable numerical method. The numerical kernel is based on *pdelib*, an FEM and FVM toolbox developed at WIAS [3].

Figure 7: Influence of geometry on hardening profile. Simulation of electron hardening of a plate with hole parallel to the surface in 2 mm distance (left) in comparison with the corresponding experimental result (right), steel C45.

The influence of workpiece geometry on the resulting hardening profile which has already been mentioned in the introduction is reflected again in Figure 7, where the numerical simulation of electron beam hardening of a plate with hole parallel to the surface (left) is compared to the corresponding experimental result (right). One can conclude that the numerical results are in good agreement with the experiment. Further simulations and experiments have been done for a number of relevant steels, the results are documented in [1].

Now, we consider a two-dimensional example corresponding to the situation depicted in Figure 7. A laser beam with constant energy and velocity moves along the upper surface from left to right. In order to observe the developing of the hardening depth the laser beam starts in a little distance from the left edge. The resulting hardening profile and the temperature T_{hs} in the hot spot on the surface are shown in Figure 8. Because the laser beam moves with constant velocity the time coordinate for T_{hs} corresponds to the space coordinate for the hardening profile.

Initially, the temperature T_{hs} and the hardening depth increase only gradually. Above the hole and at the right-hand edge T_{hs} shows an overshooting and the hardening depth increases.

4 Feedback control of temperature

4.1 Linear PID control for laser surface hardening

4.1.1 Motivation

Owing to the results shown in Figure 8 the temperature T_{hs} in the hot spot on the surface is related to the depth of the hardening profile. In a small part between the hole and the right-hand edge (corresponding to $12s < t < 15s$) the hardening profile has a constant depth of one millimeter and the value of T_{hs} is $1360C$. Hence a reasonable strategy seems to be trying to keep the temperature T_{hs} in the hot spot

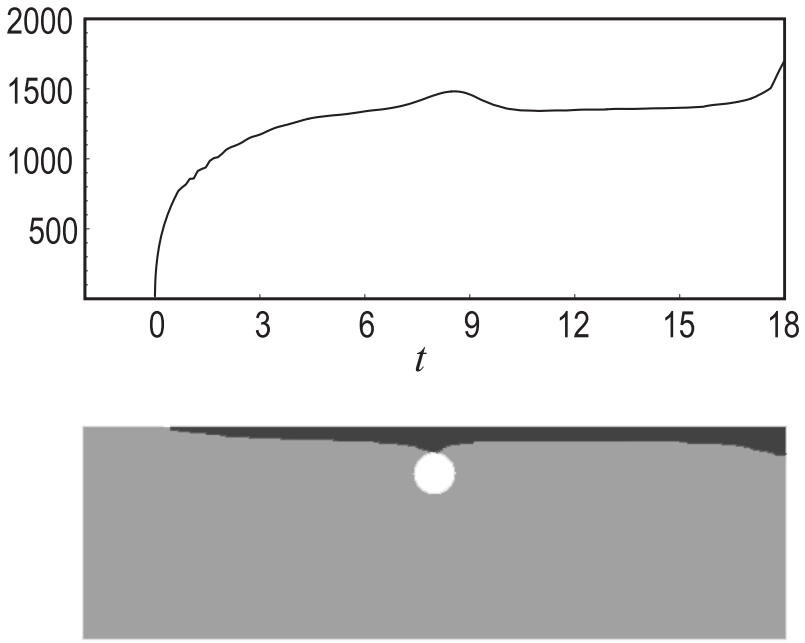

Figure 8: Results for constant laser beam power. Top: temperature T_{hs} in the hot spot on the surface. Bottom: hardening profile.

on the surface constant by controlling the power of the laser beam.

This is also possible in industrial applications where the temperature is observed by a pyrometer.

4.1.2 Algorithm I: Surface Control

The goal of this PID (short for Proportional Integral Differential) control is to adjust a desired set-point temperature $\widehat{T}$ in the hot spot of the beam focus on the workpiece surface. Let $\bar{x}(t)$ denote the location of this hot spot on the workpiece surface at time t, i.e. we have

$$T_{hs}(t) = T(\bar{x}(t), t).$$

Then we can define the difference between actual temperature and set-point temperature by

$$e(t) = \widehat{T} - T(\bar{x}(t), t).$$

We use the laser energy G (cf. (4)) as control parameter. Introducing the time discretization $0 = t_0 < t_1 < \ldots < t_N = t_E$, whe can formulate the algorithm for PID beam hardening control in the following way:

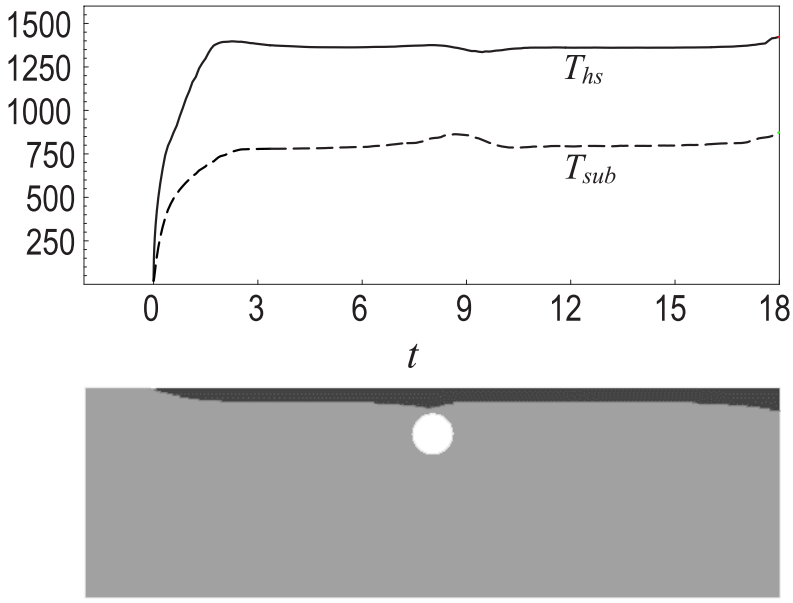

Figure 9: Linear PID control of surface temperature (Algorithm I). Top: temperature in the hot spot on the surface (continuous line) and close to the lower boundary of the hardening zone (dashed line). Bottom: hardening profile.

For $i = 0$ **to** $N - 1$ **do:**

$$e(t_i) = \widehat{T} - T((\bar{x}(t_i), t_i), \tag{5a}$$

$$G(t_{i+1}) = k_P e(t_i) + k_I \int_{t_0}^{t_i} e(t)\, dt + k_D \dot{e}(t_i) \tag{5b}$$

The three terms on the right-hand side of (5b) correspond to the proportional, integral and differential part of the PID- controller. The determination of optimal values for the constants k_P, k_I and k_D is explained in Subsection 4.1.5. Note that the integration and differentiation in (5b) have to be replaced by the corresponding discrete counterparts when coupling this algorithm with the numerical approximation of the state equations.

Now we apply *Algorithm I* to the two-dimensinal example described above. To this end we define the set-point temperature as $\widehat{T} = 1360^o C$. The result is given in Figure 9. Although the surface temperature in the hot spot of the focus is now nearly constant, the hardening profile again shows a thickening above the hole and at the edge of the plate. The reason becomes clear if one takes a look at the temperature in the lower part of the hardening strip in some distance d from the surface. Let $T_{sub}(t)$ be the maximal temperature at time t in distance d from the surface, with location $\underline{x}(t)$, i.e. we have

$$T_{sub}(t) = T(\underline{x}(t), t).$$

Note that in view of Figuere 6 $\bar{x}(t) - \underline{x}(t)$ is perpendicular to the penetrated surface

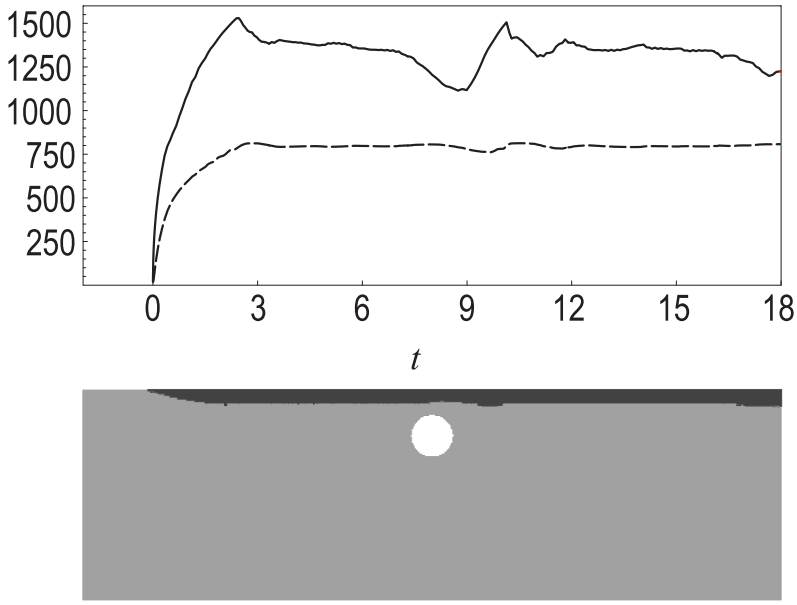

Figure 10: Linear PID control of subsurface temperature (Algorithm II). Top: temperature in the hot spot on the surface (continuous line) and close to the lower boundary of the hardening zone (dashed line). Bottom: hardening profile.

if and only if the laser is at rest, otherwise, the angle between $\bar{x}(t) - \underline{x}(t)$ and v is more than $\pi/2$.

One can see that $T_{sub}(t)$ in Figure 9 shows more or less the same behaviour as the surface temperature T_{hs} in the uncontrolled case depicted in Figure 8. Thus it might be more favourable to try to keep the temperature T_{sub} constant by controlling the laser energy.

4.1.3 Algorithm II: Subsurface Control

Now we use a temperature which is typically attained in the lower part of the hardening strip as set-point temperature. In our case we take $\widehat{T} = 800^oC$. Then the goal is to adjust $\widehat{T}$ in the hot spot in a distance d from the workpiece surface. We choose the distance d equal to the desired hardening depth, 1mm in our case. The algorithm (5) is then replaced by
For $i = 0$ **to** $N - 1$ **do:**

$$e(t_i) = \widehat{T} - T((\underline{x}(t_i), t_i), \tag{6a}$$

$$G(t_{i+1}) = k_P e(t_i) + k_I \int_{t_0}^{t_i} e(t)\, dt + k_D \dot{e}(t_i) \tag{6b}$$

The resulting hardening profile is approximately uniform as can be seen in Figure 10. The dashed line in the graph above represents the controlled temperature T_{sub}in

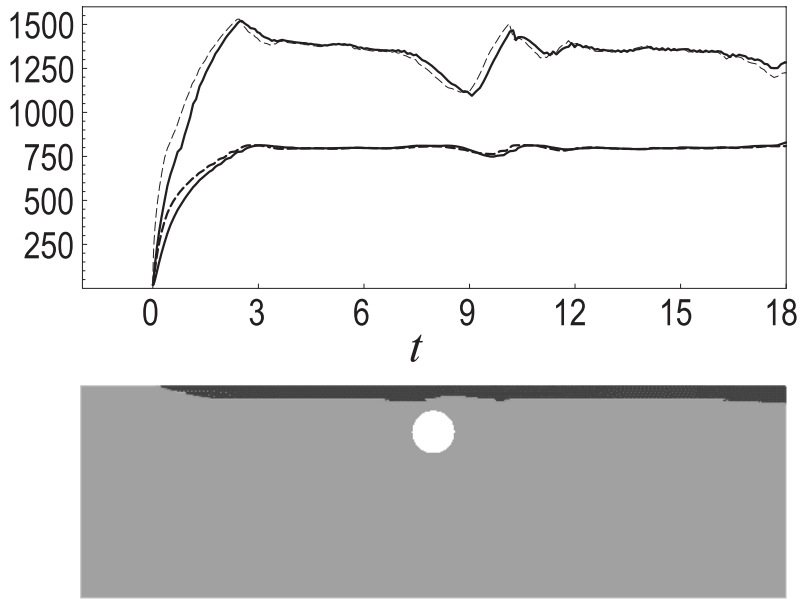

Figure 11: Linear PID control of surface temperature with set point T_{hs} from Fig. 10. Top: temperature in the hot spot on the surface and close to the lower boundary of the hardening zone (straight lines) and temperatures from Fig. 10 (dashed lines). Bottom: hardening profile.

a fixed distance from the surface, which is nearly constant now, owing to the PID-control. The continuous line depicts the surface temperature in the hot spot, which is not at all constant.

4.1.4 Utilization of subsurface control for the process control of the hardening machine

In the real hardening process it is not possible to observe the temperature T_{sub} in some fixed distance below the surface and hence it is impossible to control the subsurface temperature. On the other hand, we have just computed the optimal temperature T_{hs}^{opt} corresponding to a uniform hardening depth as a by-product when applying *Algorithm II* for subsurface control (the continuous line in Figure 10). Thus we propose to use T_{hs}^{opt} as the set-point for the pyrometer process control.

To demonstrate that this is a promising approach, we define

$$\widehat{T}(t) = T_{hs}^{opt}(t)$$

and apply again *Algorithm I* for surface control. The results can be found in Figure 11. The continues lines correspond to the resulting temperatures T_{hs} and T_{sub} while the dashed lines correspond to the results from the subsurface control depicted already in Figure 10. The computed surface temperature T_{hs} lags a bit behind the set-point temperature T_{hs}^{opt} but the resulting hardening profile is nearly as uniform as the one in Figure 10.

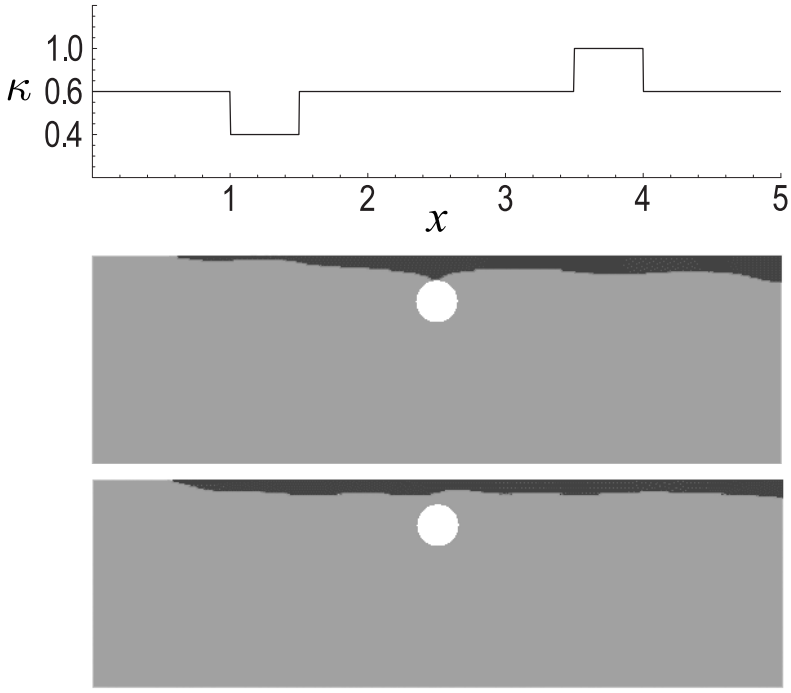

Figure 12: Simulation with varying absorption coefficient. Top: absorption coefficient. Center: hardening profile for constant laser power. Bottom: hardening profile resulting from Algorithm I with T_{hs}^{opt} as set-point temperature.

As a second verification we now consider the case of a space dependent absorption coefficient κ. One reason, why temperature control is such an important issue for the laser hardening process is that the surface conditions may vary in the area to be hardened, e.g., due to varying roughness, shading or grease spots. Although the absorption coefficient is not constant in this case, the optimal temperature in the hot spot on the workpiece surface should still be the same. Figure 12 shows the numerical simulation of such a situation. On top one can see the space-dependent absorption coefficient. Below is the resulting hardening profile in the case of constant laser energy. One can see that the hardness decreases in regions where the absorption coefficient decreases and vice versa. At the bottom the hardening profile is shown which again results from the application of *Algorithm I* for suface control with set-point temperature $\widehat{T}(t) = T_{hs}^{opt}(t)$ where T_{hs}^{opt} stems from the application of *Algorithm II* for subsurface control. Again, the resulting hardening profile is nearly as uniform as the one in Figure 10.

4.1.5 Controllability and parameter tuning

For the simulations mentioned above the control parameter for the PID algorithm, k_P, k_I and k_D, have to be determined. The tuning of these parameters is based on a step response of the system. Figure 13 shows the temperature T_{hs} and T_{sub} corresponding to a stepwise jump in laser power. There is hardly any lag in the step

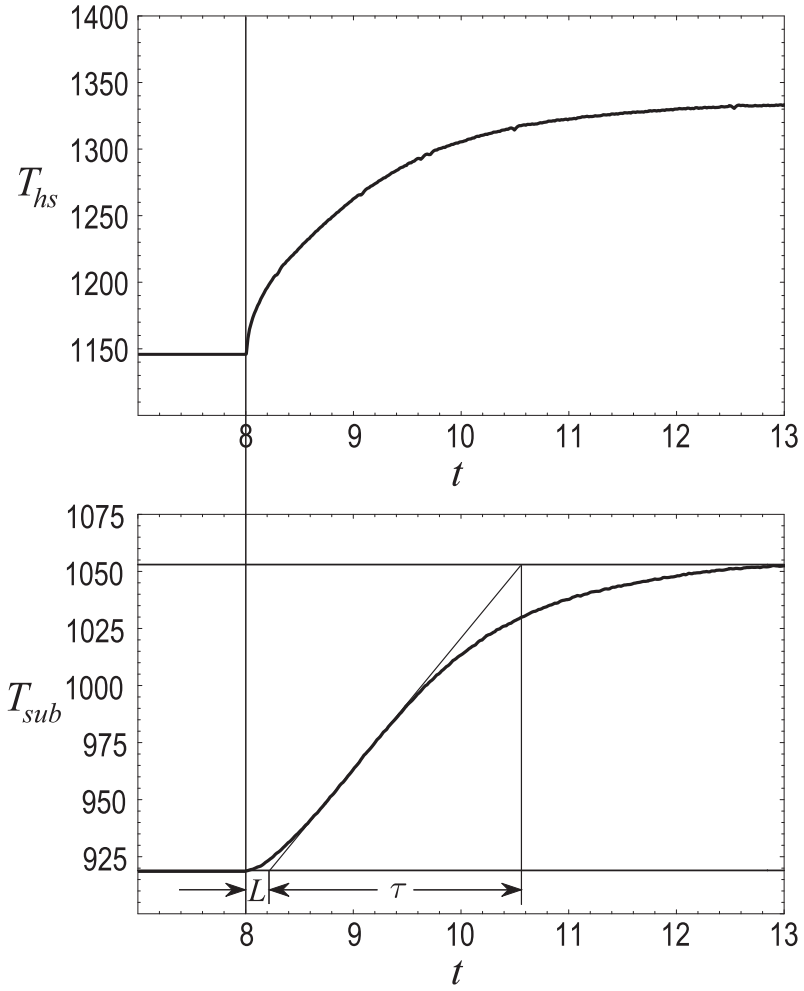

Figure 13: Response to a stepwise jump in laser power. Top: temperature in the hot spot on the surface. Bottom: temperature close to the lower boundary of the hardening zone .

response of the surface temperature and therefore T_{hs} should be well controllable by the PID algorithm. However, this is not the case for the temperature T_{sub} close to the lower boundary of the hardening zone. The lag L increases with the velocity of the laser beam. Since the characteristic time constant τ of the process is hardly influenced by the velocity of the laser beam, the ratio τ/L decreases if v increases and above a certain velocity the controllability of T_{sub} by the PID algorithm becomes rather poor. In our simulations the critical velocity of the laser beam turns out to be $0.25cm/s$ for a hardening depth of one millimeter. This corresponds nicely to the the relationship between hardening depth d and laser velocity as depicted in Figure 6. For smaller hardening depths the critical velocity increases.

To determine the three PID parameters we have used the tuning rules by Ziegler and Nichols [9]. In addition we have tried the rules by Chien, Hrones and Reswick [9], but the differences in the resulting hardening profiles have not been found very significant.

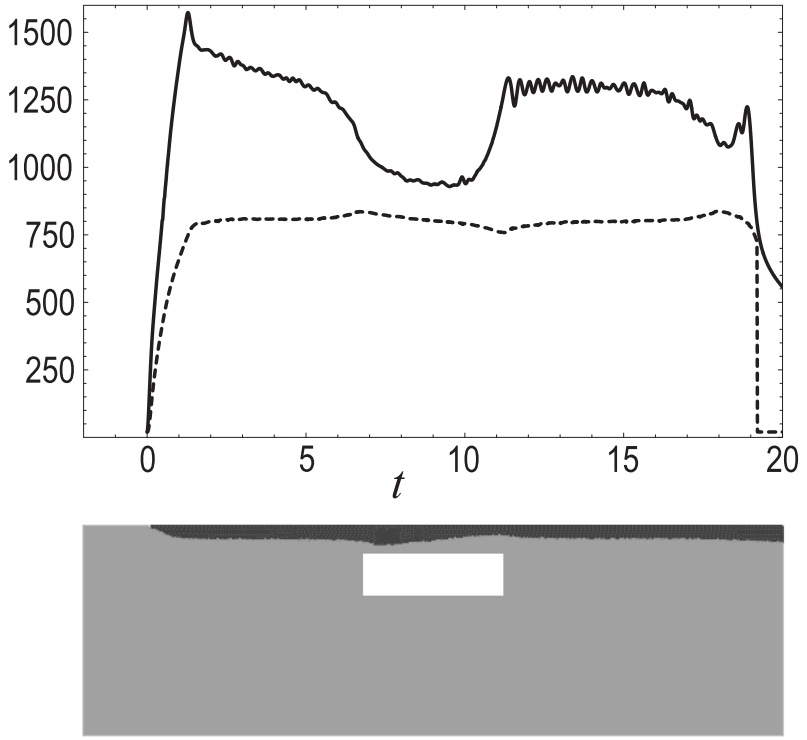

Figure 14: Linear PID control of subsurface temperature (Algorithm II). Top: temperature in the hot spot on the surface (continuous line) and close to the lower boundary of the hardening zone (dashed line). Bottom: hardening profile.

4.2 Nonlinear PID control

Unfortunately, our linear PID approach fails in the case of workpices with more complicated geometries, for example, if the circular hole is replaced by a rectangular one. Figure 14 shows the results of *Algorithm II* applied to such a case. The algorithm fails to keep T_{sub} constant above the hole and the resulting hardening strip is not uniform above the hole.

In order to improve the results obtained with the linear PID algorithm, we replace (5b) and (6b), respectively, with the nonlinear equation

$$G(t_{i+1}) = k_P e(t_i) + k_1 \arctan(k_2 e(t_i)) + k_I \int_{t_0}^{t_i} e(t)\,dt + k_D \dot{e}(t_i), \tag{7}$$

with two additional parameter k_1 and k_2. For $k_1 = 0$ we recover the usual linear PID algorithm. Due to the nonlinear term the modified PID algorithm is very sensitive to small errors $e(t)$. The advantage of similar nonlinear terms in the PID algorithm is pointed out in [4]. Up to now we have no tuning rules for k_1 and k_2. Therefore k_1 and k_2 are adjusted by hand.

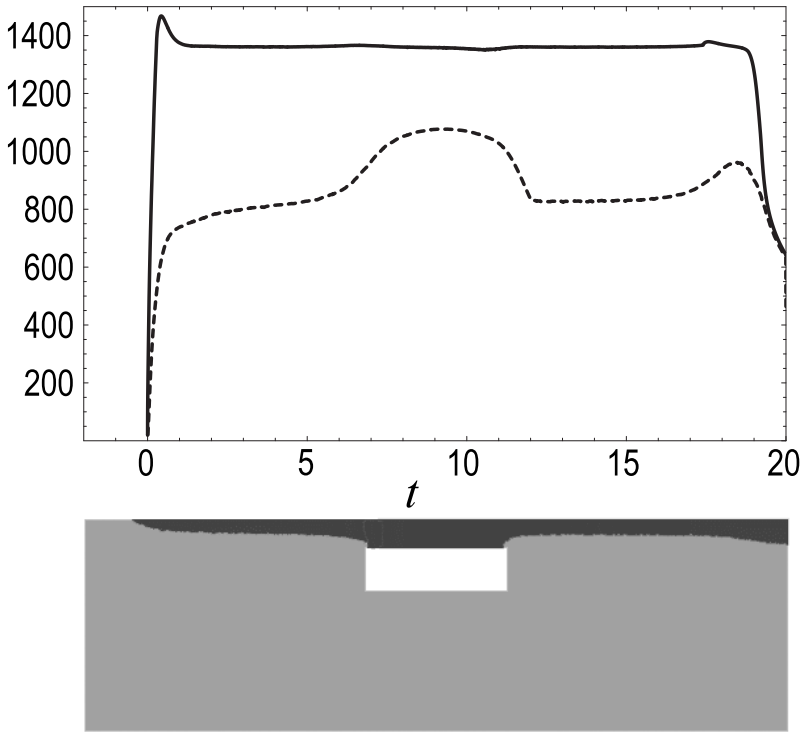

Figure 15: Nonlinear PID control of surface temperature. Top: temperature in the hot spot on the surface (continuous line) and close to the lower boundary of the hardening zone (dashed line). Bottom: hardening profile.

Now we again define the set-point temperature $\widehat{T} = 1360^oC$ and apply *Algorithm I* for surface control, but with (5b) replaced with (7). The results are depicted in figure 15. We obtain a nearly constant temperature T_{hs}. However, although T_{hs} is constant, the temperature T_{sub} is not and the hardening profile shows an increase in thickness avove the hole and at the end.

Figure 16 shows the results of the application of *Algorithm II* for subsurface control, where (6b) has been replaced with its nonlinear counterpart (7) and a set-point temperature $\widehat{T} = A_s = 800^oC$ has been chosen. The resulting subsurface temperature T_{sub} is nearly constant and therefore also the depth of the hardening profile. However, as in Subsection 4.1.3 the corresponding temperature in the hot spot T_{hs} on the surface is no longer constant. It may serve as a set-point in a real hardening process in which it is possible to control T_{hs} by pyrometer technique.

Also for the workpice with the circular hole the algorithm (7) works very well. Hence we recommend to use the nonlinear PID version (7) for surface hardening control.

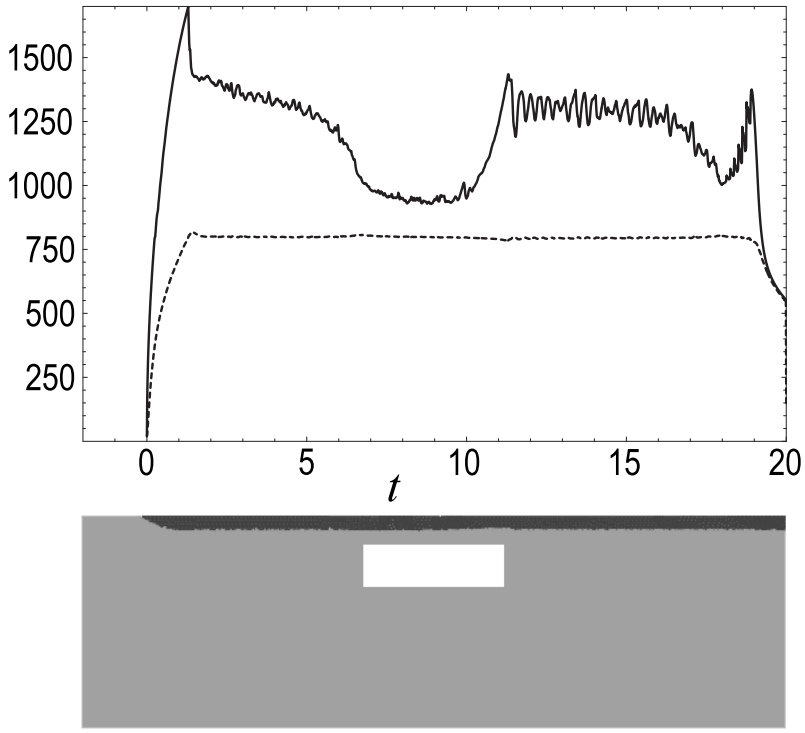

Figure 16: Nonlinear PID control of subsurface temperature. Top: temperature in the hot spot on the surface (continuous line) and close to the lower boundary of the hardening zone (dashed line). Bottom: hardening profile.

5 Concluding remarks

The goal of process control for laser hardening is twofold. On the one hand a melting of the surface has to be avoided to maintain the workpiece quality. On the other hand, only a uniform thin layer should be hardened to reduce fatigue effects. While the former can be achieved with a control of surface temperature and hence can be realized by machine process control, the latter one cannot (cf. Figure 15).

A uniform hardening depth can only be achieved by subsurface temperature control. To achieve this goal numerical simulations are indispensable. As we have shown the resulting non-constant surface temperature may be used as a set-point for the machine proces control.

Finally, we would like to remark that all the numerical simulations in this paper have been carried out for the steel CK45. For other steels the set-point temperatures have to be changed accordingly. More precisely, we would recommend to define $T_{hs} = T_{melt} - 50^oC$, where T_{melt} is the melting temperature for the required steel, and $T_{sub} = A_s$.

References

[1] A. Buchwalder and other. Simulation der Strahlhärtung von Stahl mit *WIAS-SHarP*. Technical Report 3, WIAS, 2002.

[2] J. Fuhrmann and D. Hömberg. Numerical simulation of surface heat treatments. *Num. Meth. Heat & Fluid Flow*, 9:705–724, 1999.

[3] J. Fuhrmann, T. Koprucki, and H. Langmach. pdelib: An open modular tool box for the numerical solution of partial differential equations. design patterns. In *14th GAMM Seminar Kiel on Concepts of Numerical Software*, 1998.

[4] Z. Gao. From linear to nonlinear control means: a practical progression. *ISA Transactions*, 41:177–189, 2002.

[5] H.E. H.E. Cline and T.A. Anthony. Heat treating and melting material with a laser or electron beam. *J. Appl. Phys.*, (48):3895–3900, 1977.

[6] D. Hömberg. Irreversible phase transitions in steel. *Math. Methods Appl. Sci.*, 20:59–77, 1997.

[7] D.P. Koistinen and R.E. Marburger. A general equation prescribing the extent of the austenite-martensite transformation in pure iron-carbon alloys and plain carbon steels. *Acta Met.*, 7:59–60, 1959.

[8] J.-B. Leblond and J. Devaux. A new kinetic model for anisothermal metallurgical transformations in steels including effect of austenite grain size. *Acta Met*, 32:137–146, 1984.

[9] W.S. Levine. *The control handbook*. CRC Press, Boca Raton, USA, 1996.